APEM journal
Advances in Production Engineering & Management
Volume 11 | Number 1 | March 2016 | pp 29–37
http://dx.doi.org/10.14743/apem2016.1.207
ISSN 1854-6250
Journal home: apem-journal.org
Original scientific paper

Thermal analysis on a weld joint of aluminium alloy in gas metal arc welding

Ismail, M.I.S.[a,*], **Afieq, W.M.**[a]

[a]Department of Mechanical and Manufacturing Engineering, Faculty of Engineering, Universiti Putra Malaysia, Serdang, 43400, Selangor, Malaysia

ABSTRACT

In this paper, a three-dimensional finite element model has been developed to simulate dynamically the gas metal arc welding (GMAW) process of aluminium alloy sheets. The numerical simulation was conducted using a non-linear transient thermal analysis by changing the welding parameters: namely arc power and welding speed. A moving Gaussian distributed heat source is implemented. All major physical phenomena associated with the GMAW process, such as thermal conduction and convection heat losses are taken into account in the model development. The developed model can calculate the temperature field and predict the weld geometry profile during the welding process. The measurement of weld bead profile from the GMAW experiments was used to validate the developed finite element model. The numerical study reveals that the arc voltage and welding speed have a significant influence on the temperature distribution, weld pool size and shape, and weld bead geometry. The results show that there are good agreements with the weld bead profile between the experimental observation and finite element simulation.

ARTICLE INFO

Keywords:
Gas metal arc welding
Aluminium alloy
Weld bead profile
Finite element model
Thermal analysis

**Corresponding author:*
ms_idris@upm.edu.my
(Ismail, M.I.S.)

Article history:
Received 31 August 2015
Revised 22 January 2016
Accepted 25 January 2016

1. Introduction

Welding ranks high among industrial processes and involves more sciences and variables than those involves in any other industrial process. Today, the welding has four popular processes, which are shielded metal arc welding (SMAW), metal inert gas (MIG), flux core arc welding (FCAW) and tungsten inert gas welding (TIG). MIG welding is one of the gas metal arc welding (GMAW) subtypes which are a welding process that joint two or more parts by melting the filler with the similar type of material of the product. The purpose of the shielding gas during the MIG welding is to protect the process from the contaminants in the air.

The quality of this welding process can also refer to the formation of the welding bead profile. However, the size of welding bead is hard to predict and to measure where it is depend on the power usage and the speed of welding [1, 2]. Experimental work can be one of the techniques to measure welding bead profile from a set of parameter [3, 4]. However, experimental trials have some uncertainties in the data obtained [5]. By doing the experimental work, the heat data that had been generated during the welding process could not be generated. The weld bead also can be predicted by using mathematical approaches [6-9]. Nevertheless, the main disadvantage of the mathematical model, it does not consider the variation of the thermal properties with temperature, which has very little practical or theoretical relevance to describe the real GMAW process.

Thermal analysis is very important to conduct the numerical simulation for welding process [10-12]. Simulation of welding process first appeared in early 1970's, and comprehensive review regarding developments in the welding simulation is by Lindgren [13-15]. Ueda and Yamakawa [16] and Hibbitt and Marcal [17] are among the pioneers who initiated application of finite element technique on simulation of welding. Goldak et al. [18] presented a so-called double ellipsiodal heat source model which is having Gaussian distribution of power density in space. There are many research papers successfully utilized the numerical simulation in the research and development of arc welding [19, 20], friction stir welding [21], laser beam welding [22], and electron beam welding [23], which deal with the temperature field and weld bead geometry of welding by using numerical models. By carrying out the thermal analysis using the finite element method, the thermal field data could easily be generated. Moreover, the weld bead size could also be easily measured by measuring the area of melting point of material.

In this study, the MIG welding process was investigated through finite element analysis. A three-dimensional finite element model has been developed to simulate the MIG welding process. The effect of heat input on MIG welding process also has been study in this project. In order to validate the finite element model, the experimental work of MIG welding process of thin plate aluminium alloy AA6061 was carried out to investigate the welding bead profile. The weld bead geometry was measured at different power input and welding speed.

2. Finite element model

2.1 Heat transfer analysis

The transient temperature field of the welded specimen is a function of time t and Cartesian coordinate system with y-axis along the welding direction, z-axis along the thickness direction and the origin locating on the specimen on the specimen surface. The governing equation for the transient heat conduction can be expressed as Eq. 1:

$$\rho c \frac{\delta \theta}{\delta t} = k\left(\frac{\delta^2 \theta}{\delta x^2} + \frac{\delta^2 \theta}{\delta y^2} + \frac{\delta^2 \theta}{\delta z^2}\right) + Q \tag{1}$$

where θ is the temperature, ρ is the material density, c is the specific heat, k is the thermal conductivity, and Q is the internal heat generation per unit volume. The thermal analysis was conducted using temperature dependent thermal material properties as shown in Fig. 1, which were taken from Afieq [24].

In this study, the heat source can be modelled by using Gaussian distribution at any time t, for the heat source of welding arc. The points that are lying on the surface of the specimen are within the arc radius r_a receive distribution of heat flux $q(t)$ according to the Eq. 2 [25],

$$q(t) = \frac{3Q_A}{\pi {r_a}^2} exp\left[-\left(\frac{r(t)}{r_a}\right)^2\right] \tag{2}$$

where $r(t)$ is the radial distance measured from the arc centre of the specimen, and Q_A is the total heat input of the welding process, and it can be written as Eq. 3,

$$Q_A = \eta VI \tag{3}$$

where Q_A is the heat input, V is the voltage, and I is the current radius. The efficiency η value for this welding process is 0.9 due to GMAW process [26].

The boundary condition of the heat transfer Eq. 1 was assumed as the heat flux generated by the welding arc, which is only applied on the top surface of the specimen and is defined by Eq. 2. While, on the non-welded top surface, the heat flux was assumed to be only the convective heat flux q_c, and can be expressed as $q_c = h_c\,(\theta - \theta_0)$, where h_c is the coefficient of the heat convection

(h_c = 10 W/m²K) [27, 28] and θ_0 is the room temperature of the surrounding environment. The initial temperature of specimen was also assumed as θ_0.

In order to obtain the solution to the thermal equilibrium equation, the initial and boundary conditions are needed. The finite element equation for the thermal analysis can be expressed as follows:

$$[C]\{\dot{\theta}\} + [K]\{\theta\} = \{Q\} \tag{4}$$

where $[C]$, $[K]$, $\{Q\}$, $\{\theta\}$ and $\{\dot{\theta}\}$ are heat capacity matrix, heat conduction matrix, heat flux column, nodal temperature column and nodal temperature rate column, respectively.

2.2 Model development

A three-dimensional (3D) finite element model was developed using ANSYS finite element software. The model was created under the similar dimension with the specimen of experimental work. It has 100 mm in width, 125 mm in length and 3 mm in thickness. The mesh was graded finest in the region of highest and most rapid temperature gradient near the heat input, and a coarse mesh was used outside the heating zone as illustrated in Fig. 2. The mesh generation was carried out first on the upper or lower surface of the specimen. Then, 3D mesh was generated by taking offsets across the specimen thickness. In order to capture the characteristics of GMAW process accurately, the mesh size increases exponentially across the thickness of the specimen, being finer near the heated side of the specimen. The mesh was composed of a total number of 29312 elements. The elements were the thermal analysis element PLANE77 and SOLID70 for 2D eight-node thermal solid and 3D eight-node thermal solid, respectively. The extrapolation method which was established by Richardson in 1926 and widely used for assessing the solution accuracy of many problems in finite volumes [29-31] and finite elements [32, 33] analyses. However, in the numerical modeling of welding process, the accuracy of mesh size has been proposed by Moraitis and Labeas [34] and Malik et al. [35]. In this method, the peak temperature is the parameter being studied in sensitivity analysis of the mesh size. Application of a finer mesh in this work led to less than 2% difference in the peak temperatures. Therefore, the presented mesh was used. An ANSYS Parametric Design Language (APDL) was used to model the moving heat source. The distributed heat flux moves with time. When the distributed heat flux moves to the next step, the former distributed heat flux step is deleted. In the present case, a moving laser beam heat source with small steps is adopted in order to simulate its continuous scanning.

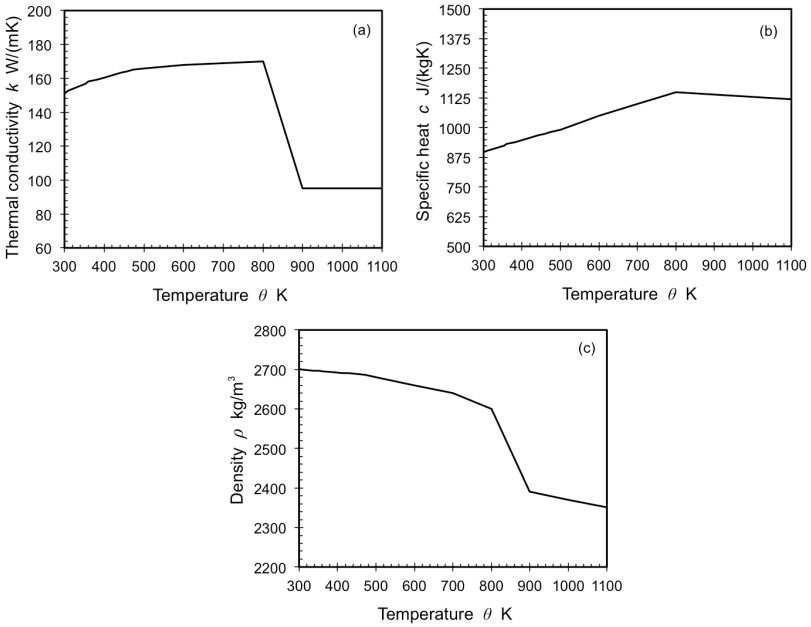

Fig. 1 Thermophysical properties of aluminium alloy AA6061

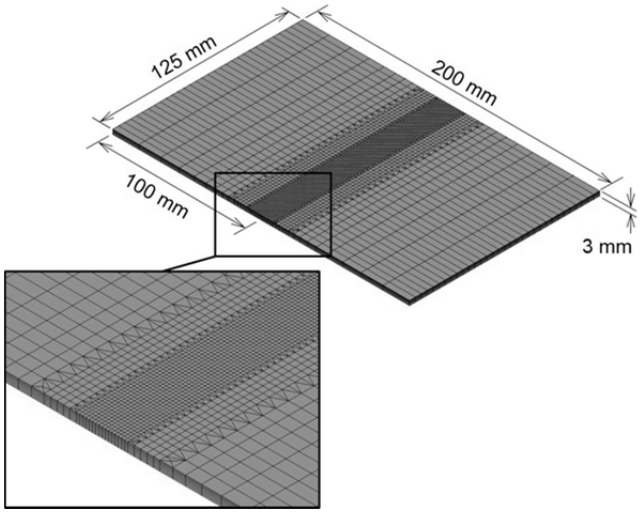

Fig. 2 Finite element model of gas metal arc welding process

3. Experimental work

A schematic diagram of experimental setup is shown in Fig. 3. In this study, the GMAW process was performed by using KempoWeld machine with 1 mm aluminium wire electrode under a shielding gas of argon. The orientation of welding torch was aligned 45 degree to the perpendicular axis of specimen top surface. The welding experiments were carried out with a motorize translations stage to execute the consistent welding speed. The workpiece material used in this study was aluminium alloy AA6061. The chemical composition is listed in Table 1. The aluminium alloy with thickness of 3 mm was cut to two plates of 100 mm x 125 mm. The butt-joint weld design was welded as shown in Fig. 3.

Welding experiments were conducted according to welding conditions as shown in Table 2. The selected welding speeds were 30 mm/s and 40 mm/s. The arc voltage were varied from 18 V to 22 V. Welding current, wire electrode feed rate and flow rate of shielding gas remained constant throughout the experiment. After the welding process, the welded specimens were cut perpendicular to the welding direction for the observation of weld bead by optical microscope.

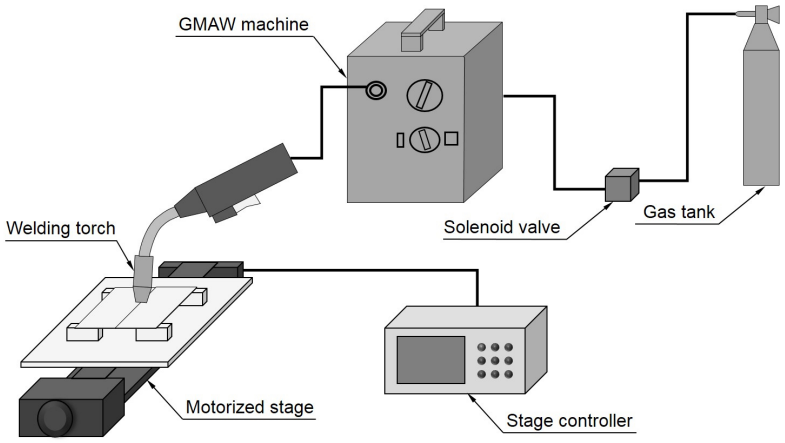

Fig. 3 Schematic diagram of experimental setup

Table 1 Chemical composition of aluminium alloy AA6061 (wt.%)

Al	Cu	Fe	Mg	Mn	Si	Ti	Zn
Bal.	0.15	≤0.7	0.8-1.2	0.15	0.4-0.8	0.15	0.25

Table 2 Welding condition

Parameter	Value
Welding speed (mm/s)	30, 40
Welding voltage (V)	18, 20, 22
Welding current (A)	140
Flow rate (l/min)	18
Shielding gas	Argon
Wire electrode feed rate (mm/s)	148
Wire electrode diameter (mm)	1

4. Results and discussion

Fig. 4 shows the temperature distribution at the top surface of the cross-section of the specimen along the welding path along *x*-axis for the 22 V welding power and 30 mm/s welding speed at the location of 94 mm from the starting point (x = 0 mm). The iteration time of each step for this analysis is 0.033 mm/s due to the welding speed. The temperature on the surface along the welding path is increasing rapidly after it is been heated by the welding arc, where the heat is then distributed throughout the plate. In this analysis, the cooling process has immediately taken place after the welding has finish at 5.17 s where it undergoes convection of heat transfer on the surface. The highest reading of temperature heating the plate almost reaches 8000 K where it is located on the centre of the arc. The convection of heat transfer are taken place during the welding process where there are difference in temperature reading where the highest reading is on the arc location, meanwhile the temperature at locations which already undergo the welding process are already slightly reduced.

Fig. 5 shows the temperature histories for three points located transversally to the weld direction. The peak temperature is at the "heel" of the center of the welding arc. In this period, the peak temperature remains constant and already in the quasi-steady state. For the same period, the velocity of the rising temperature decreases at the bottom surface as shown in Fig. 6. Since the temperature at the top surface is much higher than that at the bottom surface, the larger temperature difference between the top and bottom surfaces leads to a high temperature gradient. This significant temperature difference through the specimen thickness can also affect the final deformation of the specimen [36].

Fig. 7 shows the temperature field of heating phase and cooling phase in the welding process. The time period of heating during welding process for this parameter only takes 5.17 s which then the cooling process are taken place immediately. The heat from the heat source is distributed through the plate by the heat conduction. The temperature reading during the heating phase becomes stable when the welding process reaches the middle location of the plate on the welding path. The heat are been removed to the surrounding during the cooling phase by the heat convection process where the plate are been left at the room temperature for the cooling process.

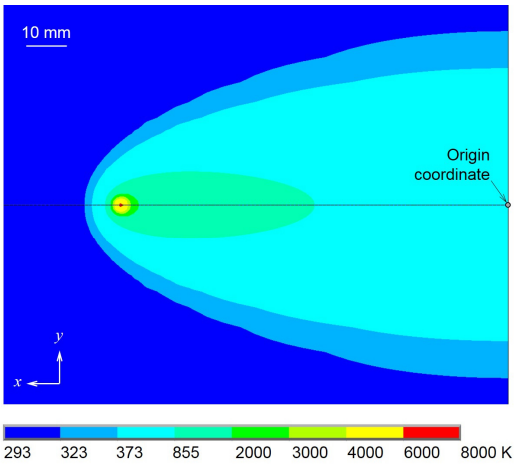

Fig. 4 Temperature distribution at the top surface along the weld direction (Voltage: 22 V, Speed: 30 mm/s)

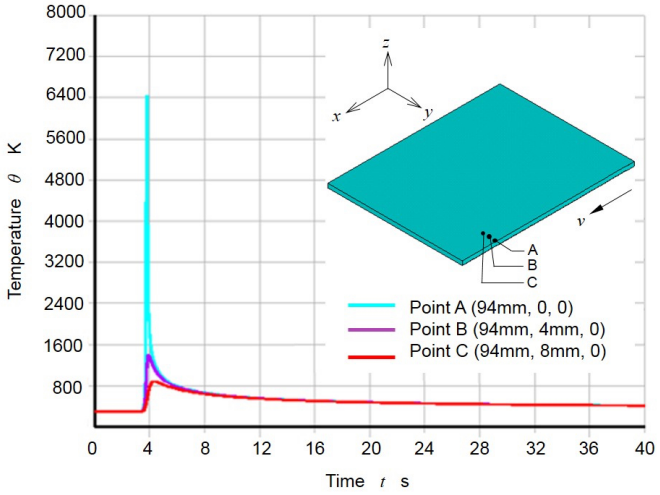

Fig. 5 Temperature histories of the three evaluated points transverse to the direction (Voltage: 22 V, Speed: 30 mm/s)

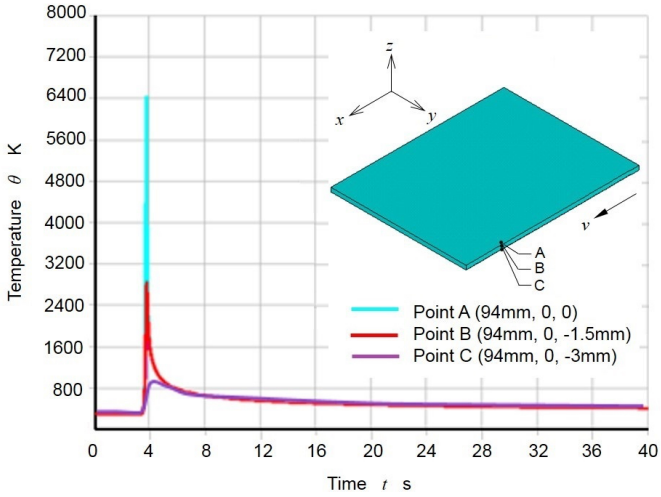

Fig. 6 Temperature histories of the three evaluated points of the cross-section of plate (Voltage: 22 V, Speed: 30 mm/s)

In Fig. 8, by having different heat input even though the similar welding speed is used due to different in the welding voltage during the welding process. The faster the welding is having lower heat input compare to the slower welding speed which is having higher heat input. This is because the welding speed is inversely proportional with the heat input. The different in the temperature distribution can be only seen on the top surface of the plate since the heat are been distributed throughout a large volume. The depth of the penetration for all parameter are similar due to the plate are thin, which the heat only throughout small volume.

In order to verify the developed model, the simulation and experimental weld geometry were compared. Fig. 9 shows the comparison of bead profile between the simulation and experimental. From this comparison, the highest heat input makes the bead formation wider when comparing parameter used in the similar welding speed. Whereas at a higher speed with the similar power usage the bead was reduce in its size. The bead profile from the experimental was viewed by using optical microscope. The height of the bump of the welding bead depended on the voltage usage and the speed of welding. The voltage of 18 V showed the highest bump formation for each speed. This was due to the low power usage to melt the filler so that it could bond completely with the plate. The usage of voltage 20 V and 22 V showed that the bump formations were smaller in sizes where the filler was completely bonded with the plate. Thus those power were more preferable to be used since the quality of welding process was been referred by the formation of bumps.

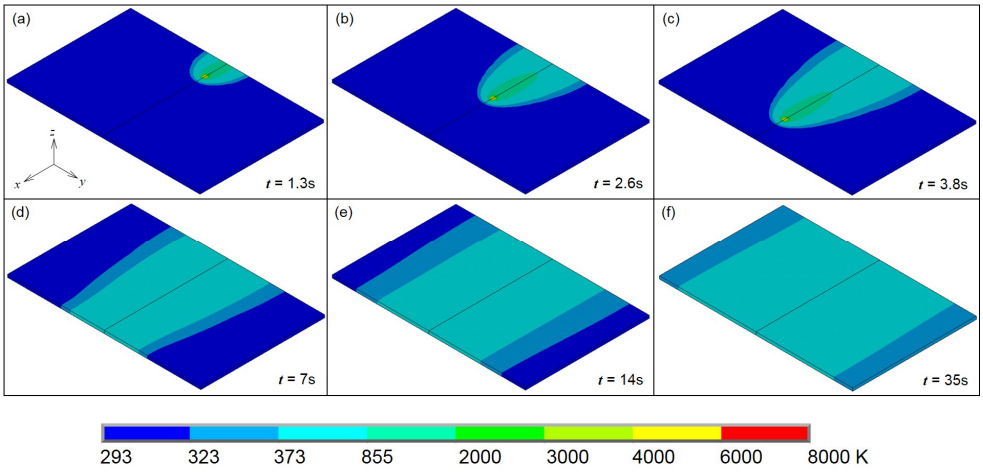

Fig. 7 Temperature distributions during welding (a-c) and cooling (d-f) (Voltage: 22 V, Speed: 30 mm/s)

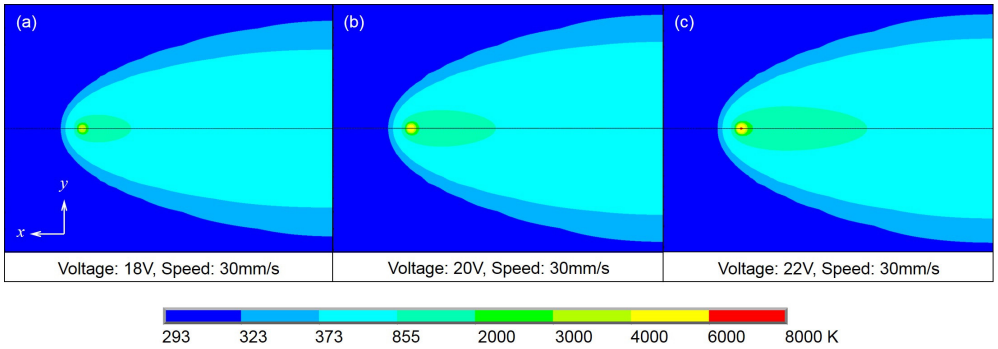

Fig. 8 Temperature distributions for welding conditions with the speed of 30 mm/s and different voltage of (a) 18 V, (b) 20 V, and (c) 22 V

Most of the percentage of error is less than 20 % and the least error is at the voltage of 18 V speed of 40 mm/s with the percentage of error of 0.05 %. The results from the analysis become the theoretical result which was used as the reference to calculate the percentage of errors. The percentage of error varies among the parameter due to some problems that occurred during the experimental which affect the results.

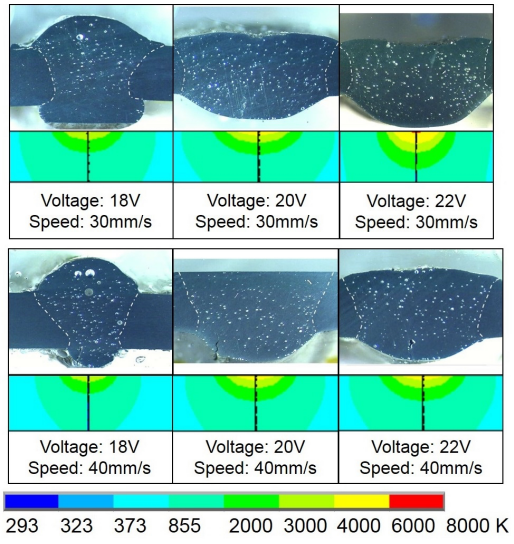

Fig. 9 Comparison between experimental and simulated weld bead profiles

The voltage that was used during the welding process may differ from the analysis since the welding machine could not maintain the power output. The power used during the welding was set by setting the arc voltage with the tolerance of ± 1 V so that the result could be acceptable. The welding process was done manually where the height of the nozzle was not static, affecting the torch arc diameter which lead to the error in the size of bead.

5. Conclusion

A three-dimensional finite element model has been developed to simulate the thermal history during gas metal arc welding of aluminium alloy sheet. Main conclusions obtained in this study are as follows:

- The developed numerical model using a Gaussian heat source can well represent the real welding as the heat source penetrates into the material.
- Arc voltage and welding speed have a significant effect on the temperature distribution, weld pool size and shape, and weld bead geometry.
- Heat input to the weld pool is transferred rapidly first in the thickness direction of the sheet and then in the width direction to reach uniformed distribution.
- Temperature distributions obtained from the developed model can be used as inputs for the thermo-mechanical analysis of aluminium alloy in gas metal arc welding.

Acknowledgement

The authors would like to acknowledge the technical support provided by Mr. Mohd Saiful Azuar Md. Isa in carrying out the experimental work at the Faculty of Engineering, Universiti Putra Malaysia (UPM).

References

[1] Benyounis, K.Y., Olabi, A.G., Hashmi, M.S.J. (2005). Effect of laser welding parameters on the heat input and weld-bead profile, *Journal of Materials Processing Technology*, Vol. 164-165, 978-985, doi: 10.1016/j.jmatprotec.2005.02.060.

[2] Shanmugam, N.S., Buvanashekaran, G., Sankaranarayasamy, K., Kumar, S.R. (2010). A transient finite element simulation of the temperature and bead profiles of T-joint laser weld, *Materials & Design*, Vol. 31, No. 9, 4528-4542, doi: 10.1016/j.matdes.2010.03.057.

[3] Talabi, S.I., Owolabi, O.B., Adebisi, J.A., Yahaya, T. (2014). Effect of welding variables on mechanical properties of low carbon steel welded joint, *Advances in Production Engineering & Management*, Vol. 9, No. 4, 181-186, doi: 10.14743/apem2014.4.186.

[4] Satheesh, M., Edwin Raja Dhas, J. (2014). Hybrid Taguchi method for optimizing flux cored arc weld parameters for mild steel, *Advances in Production Engineering & Management*, Vol. 9, No. 2, 95-103, doi: 10.14743/apem2014.2.179.

[5] Anca, A., Cardona, A., Risso, A., Fachinotti, V.D. (2011). Finite element modeling of welding process, *Applied Mathematical Modelling*, Vol. 35, No. 2, 688-707, doi: 10.1016/j.apm.2010.07.026.

[6] Sharma, A., Arora, N., Mishra, B. (2015). Mathematical model of bead profile in high deposition welds, *Journal of Material Processing Technology*, Vol. 220, 65-75, doi: 10.1016/j.jmatprotec.2015.01.009.

[7] Chan, B.K.H., Bibby, M.J., Yang, L.J., Chandel, R. (1993). A discussion of algorithms for representing submerged arc weld shape with workpiece edge preparation, In: *Winter Annual Meeting, Manufacturing Science and Engineering*, New Orleans, USA, 873-878.

[8] Kim, G.H., Kang, S.I., Lee, S.B. (1999). A study on the estimate of weld bead shape and the compensation of welding parameters by considering weld defects in horizontal fillet welds, In: *Third International Conference on Knowledge-based Intelligent Information Engineering Systems*, Adelaide, Australia, 212-216, doi: 10.1109/KES.1999.820157.

[9] Datta, S., Bandyopadhyay, A., Pal, P.K. (2008). Modelling and optimization of features of bead geometry including percentage dilution in submerged arc welding using mixture of fresh flux and fused slag, *The International Journal of Advanced Manufacturing Technology*, Vol. 36, No. 11, 1080-1090, doi: 10.1007/s00170-006-0917-4.

[10] Ma, J., Kong, F., Kovacevic, R. (2012). Finite-element thermal analysis of laser welding of galvanized high-strength steel in a zero-gap lap joint configuration and its experimental verification, *Materials & Design*, Vol. 36, 348-358, doi: 10.1016/j.matdes.2011.11.027.

[11] Ribic, B., Palmer, T.A., Debroy, T. (2009). Problems and issues in laser-arc hybrid welding, *International Materials Reviews*, Vol. 54, No. 4, 223-244, doi: 10.1179/174328009X411163.

[12] Uday, M., Ahmad Fauzi, M.N., Zuhailawati, H., Ismail, A.B. (2012). Thermal analysis of friction welding process in relation to the welding of YSZ-alumina composite and 6061 aluminum alloy, *Applied Surface Science*, Vol. 258, No. 20, 8264-8272, doi: 10.1016/j.apsusc.2012.05.035.

[13] Lindgren, L.E. (2001). Finite element modeling and simulation of welding – Part 1: Increased complexity, *Journal of Thermal Stresses*, Vol. 24, No. 2, 141-192, doi: 10.1080/01495730150500442.
[14] Lindgren, L.E. (2001). Finite element modeling and simulation of welding – Part 2: Improved material modeling, *Journal of Thermal Stresses*, Vol. 24, No. 3, 195-231, doi: 10.1080/014957301300006380.
[15] Lindgren, L.E. (2001). Finite element modeling and simulation of welding – Part 3: Efficiency and integration, *Journal of Thermal Stresses*, Vol. 24, No. 4, 305-334, doi: 10.1080/01495730151078117.
[16] Ueda, Y., Yamakawa, T. (1971). Analysis of thermal-elastic stress and strain during welding by finite element method, *Transactions of the Japan Welding Society*, Vol. 2, No. 2, 90-100.
[17] Hibbitt, H.D., Marcal, P.V. (1973). A numerical thermo-mechanical model for the welding and subsequent loading of fabricated structure, *Computers & Structures*, Vol. 3, No. 5, 1145-1174, doi: 10.1016/0045-7949(73)90043-6.
[18] Goldak, J., Chakravarti, A., Bibby, M. (1984). A new finite element model for welding heat sources, *Metallurgical Transactions B*, Vol. 15, No. 2, 299-305, doi: 10.1007/BF02667333.
[19] Hackmair, C., Werner, E., Pönisch, M. (2003). Application of welding simulation for chassis components within the development of manufacturing methods, *Computational Materials Science*, Vol. 28, No. 3-4, 540-547, doi:10.1016/j.commatsci.2003.08.011.
[20] Long, H., Gery, D., Carlier, A., Maropoulos, P.G. (2009). Prediction of welding distortion in butt joint of thin plates, *Materials & Design*, Vol. 30, No. 10, 4126-4135, doi: 10.1016/j.matdes.2009.05.004.
[21] Al-Badour, F., Merah, N., Shuaib, A., Bazoune, A. (2014). Thermo-mechanical finite element model of friction stir welding of dissimilar alloys, *The International Journal of Advanced Manufacturing Technology*, Vol. 72, No. 5, 607-617, doi: 10.1007/s00170-014-5680-3.
[22] Tsirkas, S.A., Papanikos, P., Kermanidis, Th. (2003). Numerical simulation of the laser welding process in butt-joint specimens, *Journal of Materials Processing Technology*, Vol. 134, No. 1, 59-69, doi: 10.1016/S0924-0136(02)00921-4.
[23] Reed, R.C., Stone, H.J., Dye, D., Roberts, S.M., McKenzie, S.G. (2000). Process modelling of the electron beam welding of aeroengine components, In: *Ninth International Symposium on Superalloys*, Pennsylvania, 665-674, doi: 10.7449/2000/Superalloys_2000_665_674.
[24] Afieq, W.M. (2015). *Thermal analysis of weld joint in GMAW process*, Bachelor dissertation, Universiti Putra Malaysia, Malaysia.
[25] Tian, L., Luo, Y., Wang, Y., Wu, X. (2014). Prediction of transverse and angular distortions of gas tungsten arc bead-on-plate welding using artificial neural network, *Materials & Design*, Vol. 54, 458-472, doi: 10.1016/j.matdes.2013.08.082.
[26] Atkins, G., Thiessen, D., Nissley, N., Adonyi, Y. (2002). Welding process effects in weldability testing of steels, *Welding Journal*, Vol. 81, No. 4, 61s-68s.
[27] Ismail, M.I.S., Okamoto, Y., Uno, Y. (2011). Numerical simulation on micro-welding of thin stainless steel sheet by fiber laser, *International Journal of Electrical Machining*, Vol. 16, 9-14.
[28] Yilbas, B.S., Akhtar, S., Shuja, S.Z. (2013). *Laser forming and welding processes*, Springer, New York, doi: 10.1007/978-3-319-00981-0.
[29] Ternik, P., Rudolf, R. (2014). Laminar forced convection heat transfer characteristics from a heated cylinder in water based nanofluids, *International Journal of Simulation Modelling*, Vol. 13, No. 3, 312-322, doi: 10.2507/IJSIMM13(3)5.271.
[30] Ternik, P., Buchmeister, J. (2015). Buoyancy-induced flow and heat transfer of power law fluids in a side heated square cavity, *International Journal of Simulation Modelling*, Vol. 14, No. 2, 238-249, doi: 10.2507/IJSIMM14(2)5.293.
[31] Ternik, P. (2015). Conduction and convection heat transfer characteristics of water-Au nanofluid in a cubic enclosure with differentially heated side walls, *International Journal of Heat and Mass Transfer*, Vol. 80, 368-375, doi: 10.1016/j.ijheatmasstransfer.2014.09.041.
[32] Lin, Q., Liu, J. (2007). Counterexamples to the asymptotic expansion of interpolation in finite elements, *Advances in Computational Mathematics*, Vol. 27, No. 2, 167-177, doi: 10.1007/s10444-007-9030-y.
[33] Asadzadeh, M., Schatz, A.H., Wendland, W. (2009). A new approach to Richardson extrapolation in the finite element method for second order elliptic problems, *Mathematics of Computation*, Vol. 78, 1951-1973, doi: 10.1090/S0025-5718-09-02241-8.
[34] Moraitis, G.A., Labeas, G.N. (2008). Residual stress and distortion calculation of laser beam welding for aluminum lap joints, *Journal of Materials Processing Technology*, Vol. 198, No. 1-2, 260-269, doi: 10.1016/j.jmatprotec.2007.07.013.
[35] Malik, A.M., Qureshi, E.M., Dar, N.U., Khan, I. (2008). Analysis of circumferentially arc welded thin-walled cylinders to investigate the residual stress fields, *Thin-Walled Structure*, Vol. 46, No. 12, 1391-1401, doi: 10.1016/j.tws.2008.03.011.
[36] Mandal, N.R. (2004). *Welding and distortion control*, Alpha Science International Ltd, Pangbourne, England.